ACS APPLIED MATERIALS & INTERFACES

Research Article

www.acsami.org

Nanostructured Hybrid Shells of r-GO/AuNP/*m*-TiO_2 as Highly Active Photocatalysts

Minggui Wang,[†] Jie Han,*[,†,§] Huixin Xiong,[‡] Rong Guo,[†] and Yadong Yin*[,§]

[†]School of Chemistry and Chemical Engineering, Yangzhou University, Yangzhou, Jiangsu 225002, P. R. China

[‡]School of Environmental Science and Engineering, Yangzhou University, Yangzhou, Jiangsu 225127, P. R. China

[§]Department of Chemistry, University of California, Riverside, California 92521, United States

Supporting Information

ABSTRACT: Nanostructured hybrid shells of r-GO/AuNP/*m*-TiO_2 were synthesized using SiO_2 spheres as templates, followed by graphene oxide (GO) and Au nanoparticle (AuNP) deposition and TiO_2 coating, and then post-treatments of template removal and calcination. Evaluation of their photocatalytic activity by degradation of Rhodamine B (RhB) under the irradiation of UV, visible light, and simulated daylight demonstrated the superior photocatalytic performance of the sandwich-like hollow hybrid shells, which could be attributed to the porous nature of the hybrid shells and the enhanced charge separation and visible-light absorption of r-GO and AuNPs.

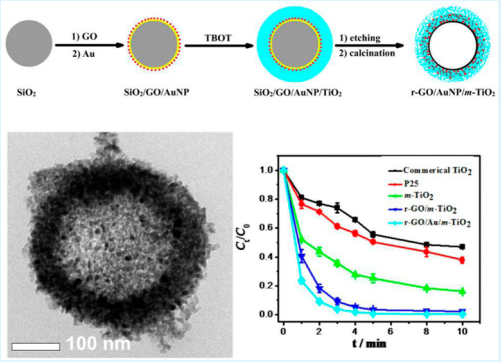

KEYWORDS: *TiO_2, graphene, Au nanoparticle, mesoporous, hybrid shells, photocatalyst*

1. INTRODUCTION

Since the discovery of its catalytic activity toward hydrogen production from water under UV light, TiO_2 has been widely studied as the most promising photocatalyst for water splitting and environmental remediation.[1−4] As a photocatalyst, TiO_2 offers a number of advantageous features, including its relatively high photocatalytic efficiency, excellent chemical stability, low toxicity, and low cost.[5,6] The development of nanoscale TiO_2 photocatalysts with suitable morphologies, such as nanorods,[7,8] nanotubes,[9] and hollow spheres,[10,11] mainly for increasing the specific surface area and enhancing the exciton transfer rate, has attracted extensive attention. Recent research has established that mesoporous hollow TiO_2 nanostructures display enhanced performance in photocatalysis because of their low density, high surface area, surface permeability, better light-trapping effect, porous characteristics, and organic adsorption.[12−16] However, the inferior utilization efficiency of visible light limits the practical photocatalytic applications of TiO_2 nanostructures due to the large band gap energy and high recombination rate of electron−hole pairs. One of the potential solutions to improve its efficiency is to shift its absorption from the UV to visible region in order to make better use of both UV and visible radiation. Various strategies, including metal ion implantation,[17] nonmetal doping,[18] and compositing with other semiconductors[19] have been extensively explored to enhance the photocatalytic activity of TiO_2 under visible light. Among them, noble metal nanoparticles such as Au and Ag have been frequently used to enhance the photocatalytic activity in visible light by taking advantage of their unique plasmonic properties.[20] In any case, improved absorption of photons may not necessarily guarantee significantly better photocatalytic performance because the efficiency of a photocatalyst is also determined by charge separation and transport.[21] Graphene nanosheets, a monolayer of carbon atoms arranged in a honeycomb network, have also been reported to hybridize with TiO_2 to slow down the recombination of photo- or electrochemically generated electron−hole pairs, enhance charge transfer rate, and increase surface adsorption of molecules to be decomposed. Generally, the enhancement of photocatalytic performance brought by graphene is attributed to its high specific surface area and superior electron mobility, which make it an ideal sink for photogenerated electrons.[22−25] It is therefore desirable to design hybrid nanostructures combining TiO_2, plasmonic metal nanoparticles, and graphene, and further explore the possible synergistic effects that may enable superior photocatalytic performances.[26,27] However, mesoporous hollow TiO_2-based ternary hybrids comprising GO and plasmonic metal nanoparticles with superior photocatalytic performances have been seldom seen.

Herein, we report the successful synthesis of sandwich-structured hybrid nanoshells containing reduced graphene oxide (r-GO), Au nanoparticles (AuNPs), and mesoporous titania (*m*-TiO_2) and demonstrate their high photocatalytic activity toward the decomposition of organic species. In this

Received: January 22, 2015
Accepted: March 12, 2015
Published: March 12, 2015

DOI: 10.1021/acsami.5b00663
ACS Appl. Mater. Interfaces 2015, 7, 6909−6918

Scheme 1. Schematic Illustration of the Synthesis Steps for r-GO/AuNP/*m*-TiO_2 Sandwich-Like Hollow Spheres

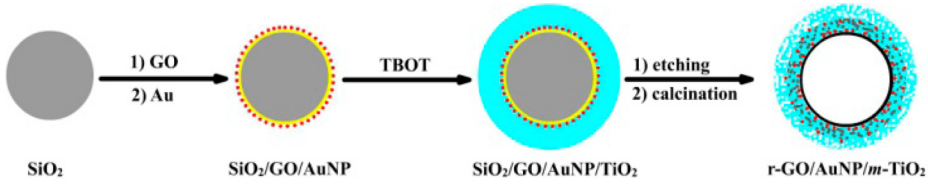

simple and scalable sol–gel based synthesis (Scheme 1), surface-modified SiO_2 spheres were used as templates, loaded sequentially with GO and AuNPs, and finally covered with a layer of TiO_2. Post-treatments including template removal and calcination led to the formation of sandwich-structured r-GO/AuNP/*m*-TiO_2 hollow shells, which possessed high surface area and exhibited excellent adsorption capability. The superior photocatalytic performance of the hybrid nanostructures was fully demonstrated in degradation of Rhodamine B (RhB) under UV light, visible light, and simulated daylight irradiations, suggesting their intriguing potential as effective photocatalysts.

2. EXPERIMENTAL METHODS

2.1. Materials. All reagents were directly used as received without further purification. Tetraethyl orthosilicate (TEOS, 99.8%), P25 (20% rutile and 80% anatase), commercial TiO_2 (99–100.5%), and 3-aminopropyltriethosysilane (APTES) (99%) were obtained from Sigma-Aldrich. Tetrabutyl orthotitanate (TOBT, 97%) was obtained from Fluka. Anhydrous ethanol, 2-propanol (99.7%), trisodium citrate dihydrate (99%), RhB, MB, and MO, graphite powder (99.85%), $KMnO_4$ (99.5%), H_3PO_4 (85%), and all other reagents were obtained from Sinopharm Chemical Reagent Co. Ltd. (China). The water used in this study was deionized by milli-Q Plus system (Millipore, France), showing 18.2 MΩ electrical resistivity.

2.2. Synthesis of GO. Typically, 0.3 g graphite and 1.8 g $KMnO_4$ were added into a mixture of 4 mL H_3PO_4 and 36 mL of concentrated H_2SO_4. After being heated to 50 °C and kept stirring for 12 h, 40 mL of ice containing 300 μL H_2O_2 was slowly added into the mixture. Then, the sample was washed with water, 3.4% HCl (aq), and ethanol by centrifugation, and then redispersed in ethanol at a concentration of 0.5 mg/mL under sonication for 24 h.

2.3. Synthesis of AuNPs. Typically, 0.24 mL of $HAuCl_4$ (0.1 mol/L) was added to 20 mL of water at room temperature (20–23 °C). After 1 min of stirring, 2.00 mL of 38.8 mmol/L sodium citrate was added. One minute later, 1.00 mL of fresh 0.075% $NaBH_4$ in 38.8 mmol/L sodium citrate was added. The colloidal solution (0.01 mol/L) was stirred for an additional 5 min and stored at 4 °C in the dark.

2.4. Synthesis and Surface Modification of SiO_2 Spheres. In a typical synthesis, 3.44 mL of TEOS was injected into a mixture of 17.2 mL of water, 2.48 mL of ammonia, and 92 mL of ethanol at room temperature under magnetic stirring. After reacting for 4 h, the colloidal spheres were collected by centrifugation and then redispersed in 10 mL ethanol. After washing twice with ethanol by centrifugation, the particles were transferred to a mixture containing isopropanol (40 mL) and APTES (300 μL) and refluxed for 3 h to functionalize the silica surface with $-NH_2$ groups. The surface modified particles were washed with ethanol and then redispersed in ethanol (2.5 mg/mL).

2.5. Synthesis of r-GO/AuNP/*m*-TiO_2 Hollow Spheres. The SiO_2/GO hybrids were fabricated simply by mixing APTES-modified SiO_2 ethanol solution and GO ethanol solution. Typically, 0.40 mL GO ethanol solution (0.5 mg/mL) was added into a 40 mL APTES-modified SiO_2 ethanol solution (2.5 mg/mL) under magnetic stirring and then the mixed solution was refluxed for 1 h. After that, SiO_2/GO hybrids were centrifuged and redispersed in 20 mL aqueous solution for further use. The SiO_2/GO/AuNP hybrids were prepared by mixing AuNP aqueous solution (1.2 mL, 0.01 mol/L) with 20 mL SiO_2/GO aqueous solution under sonication for 1 h. SiO_2/GO/AuNP hybrids were then centrifuged and washed twice with ethanol and then redispersed in 40 mL ethanol. The outer layer of TiO_2 was prepared by TBOT hydrolysis. Typically, 40 mL SiO_2/GO/AuNP ethanol solution was mixed with 0.4 mL TBOT under vigorous magnetic stirring for 1 h. Then, 20 mL water was injected into the mixture using a syringe pump at a rate of 0.5 mL/min, followed by magnetic stirring for 12 h. The as-formed SiO_2/GO/AuNP/TiO_2 hybrids were washed twice with water, redispersed in 30 mL of water under ultrasonication for 30 min, and then etched with NaOH solution (10 mL, 2.5 mol/L) at the desired temperature (90 °C) for 3 h to completely remove SiO_2 cores. After that, the solution was centrifuged and redispersed in 20 mL HCl solution (0.1 mol/L) under magnetic stirring for 1 h. Then the solution was washed twice with water and dried under vacuum. Finally, GO/AuNP/TiO_2 hybrids were calcined at 600 °C under N_2 protection for 4 h to crystallize the amorphous TiO_2 to small anatase TiO_2 grains and to change GO into r-GO through pyrolysis. The obtained r-GO/AuNP/*m*-TiO_2 hybrid hollow shells were further used as photocatalysts.

2.6. Catalytic Experiments. The photocatalytic activity was tested by degradation of RhB. Before the reaction was initiated, the catalysts were first irradiated under UV light with wavelength of 365 nm for 30 min to remove any residual organic contaminants. The catalyst (5 mg) was added to an aqueous RhB solution (25 mL, 2.0×10^{-5} mol/L) in a 50 mL quartz cell and the solution (pH = 7) was stirred in the dark for 30 min to ensure equilibrium adsorption of the dye. A UV lamp (300 W Hg) with a 365 nm filter, a visible lamp (400 W Metal Halide) with a 400 nm filter, and a sunlight simulator (350 W xenon) were used in a commercial photoreactor system (Xujiang XPA-7), the focused intensity values on the flask were 1.75 mW, 3.90 mW, and 2.01 mW, respectively. It was measured using a light dynamometer (CEL-NP2000, CEAULIGHT) with the range of 0–2000 mW. The concentration of RhB before and after irradiation was determined by measuring the absorbance at 553 nm with a UV–vis spectrophotometry (HR2000CG-UV-NIR, Ocean Optics).

2.8. Instruments. The sample morphology was characterized using transmission electron microscopy (TEM, Tecnai T12 Philip Apparatus Co., United States) and high resolution transmission electron microscopy (HRTEM, Tecnai G2 F30 S-Twin TEM, FEI). The crystal phase was evaluated by X-ray diffraction (XRD) analysis using a Bruker AXS D8 ADVANCE X-ray diffractometer. The nitrogen adsorption isotherm was obtained at 77 K using a Beishide 3H-2000PS2 specific surface and pore size analysis instrument. The surface area was calculated from the adsorption isotherm using the multipoint Brunauer–Emmett–Teller (BET) method in the pressure range of P/P_0 = 0.05–0.25. The average pore sizes were determined by the Barrett–Joyner–Halenda (BJH) method from the adsorption isotherm. The optical properties were tested by UV/vis diffuse reflectance spectra (Cary 5000, Varian). X-ray photoelectron spectroscopy (XPS) data were recorded on a PHI Quantera II using a nonmonochromatized Al Kα X-ray (1486.6 eV) as the excitation source and choosing C 1s as the reference line. The electrochemical impedance spectra (EIS) were carried out on an electrochemical workstation (PGSTAT30, Auto Lab) by using three-electrode cells. The resultant electrode served as the working electrode, with a platinum wire as the counter electrode, and a Ag/AgCl (saturated KCl) electrode as the reference electrode. The measurements were performed in the presence of a 0.5 mol/L Na_2SO_4 solution.

DOI: 10.1021/acsami.5b00663
ACS Appl. Mater. Interfaces 2015, 7, 6909–6918

3. RESULTS AND DISCUSSION

3.1. Morphology and Formation Mechanism of r-GO/AuNP/*m*-TiO_2 Hollow Spheres. Scheme 1 illustrates the synthesis steps involved in the preparation of r-GO/AuNP/*m*-TiO_2 sandwich-like hollow shells. Monodispersed SiO_2 particles were chosen as templates, followed by the self-assembly of GO on SiO_2 surfaces and further decoration of AuNPs on GO surfaces. Finally, TiO_2 layers were coated on SiO_2/GO/Au hybrid surfaces, leading to r-GO/AuNP/*m*-TiO_2 sandwich-like hollow spheres after template removal and calcination.

The apparent color changes of colloidal samples during synthesis were monitored as given in Figure S1. To ensure effective coating of GO, SiO_2 particles have been modified with a coupling agent APTES. As driven by electrostatic interactions, GO can be uniformly self-assembled onto surfaces of SiO_2 particles (Figure S2). The SEM and TEM images as given in Figure 1a and b clearly reveal the formation of SiO_2/GO core/shell hybrids. The high-resolution TEM (HRTEM) image in Figure 1b shows two or three layered GO nanosheets on surfaces of SiO_2. The subsequent step is to introduce AuNPs. There are two ways to realize the decoration of AuNPs on surfaces of SiO_2/GO hybrids: (1) the addition of presynthesized Au colloids, which can be located on surfaces of SiO_2/GO. GO, which contains carboxylic groups and π electrons, can interact with AuNPs (in addition, the remaining amino groups of modified SiO_2 may also cause adsorption of AuNPs on surfaces of SiO_2/GO); (2) the addition of $HAuCl_4$, which can result in the formation of AuNPs on the surface of GO after redox reactions between GO and $AuCl_4^-$.[28] Although the latter strategy shows the obvious advantage of the simplified procedure, the size and loading amount of in situ formed AuNPs are hard to control, which makes it difficult to reveal the effect of AuNPs on their catalytic performances. Therefore, we choose the former one to introduce AuNPs with predetermined size and amount. AuNPs of 5 nm in diameter were adsorbed onto the GO surface by strong chemical affinities, as determined by the color change of the original Au suspension from red to colorless under controlled centrifugation to isolate only SiO_2/GO particles. The formation of SiO_2/GO/AuNP hybrids has been further confirmed by TEM images (Figure 1c and d). Afterward, the outer amorphous TiO_2 shells have been formed through hydrolysis of TBOT. Finally, the SiO_2 cores have been thoroughly removed through the well-established etching process using concentrated NaOH solution,[14−16] and then the calcination process under N_2 ambient conditions to ensure crystallization and mesoporous shell formation of TiO_2 and the formation of r-GO derived form GO through pyrolysis.[29] As given in Figure 1e, r-GO/AuNP/*m*-TiO_2 hollow spheres can be clearly evidenced. In comparison with *m*-TiO_2 hollow spheres without GO and AuNPs synthesized using a similar strategy (Figure 1f), the dark dots mainly located in the inner surfaces of r-GO/AuNP/*m*-TiO_2 (Figure 1e) should be ascribed to AuNPs.

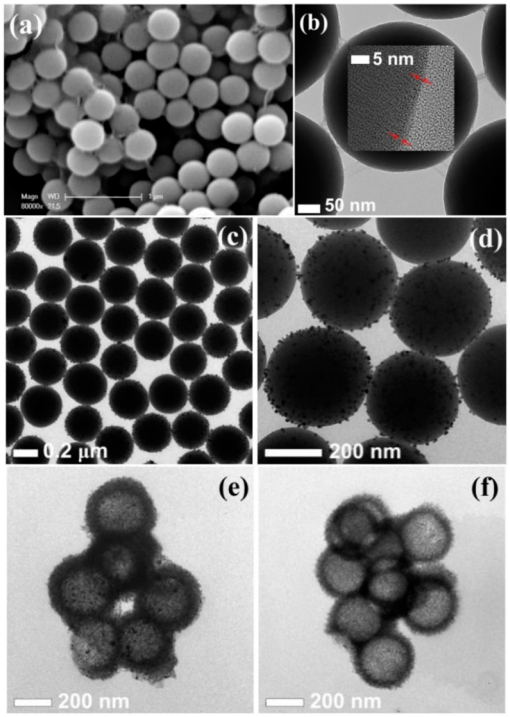

Figure 1. (a) SEM and (b) TEM images of SiO_2/GO core/shell hybrids. (c, d) TEM images of SiO_2/GO/AuNP hybrids. (e) TEM image of r-GO/AuNP/*m*-TiO_2 sandwich-like hollow shells. (f) TEM image of *m*-TiO_2 hollow shells.

In order to fully understand the sandwich-structured r-GO/AuNP/*m*-TiO_2 hollow shells, the low- and high-magnification TEM images are given in Figure 2a and b, respectively. The inner diameter is similar to the size of SiO_2 template and the mesoporous TiO_2 shell is around 50 nm in thickness. Figure 2c depicts the HRTEM image of r-GO/AuNP/*m*-TiO_2 hollow spheres. The observed fringe spacing of 0.35 nm ensures the presence of anatase TiO_2 (101) plane (JCPDS 21−1272), whereas the spacing of 0.236 nm indicates the presence of Au (111) plane (JCPDS 04−0784). The high-angle annular dark field scanning transmission electron microscopy (HAADF-STEM) image of a single r-GO/AuNP/*m*-TiO_2 particle as given in Figure 2d clearly reveals the location of AuNPs mostly on the inner surface of the TiO_2 shell. However, some AuNPs penetrating into TiO_2 porous shells can also be seen. In addition, the energy dispersive X-ray spectroscopic (EDS) elemental maps of Ti (Figure 2e), Au (Figure 2f), and C (Figure 2g) in a single shell in Figure 2d further confirm the expected structure. It should be noted that both Au and C partially penetrated into TiO_2 porous shells can be verified. As the post-treatment of calcinatin was applied to crystallize TiO_2 from amorphous into crystalline structure, the penetration of AuNPs and GO into TiO_2 shell is possibly related to the porous shell formation with voids together with high temperature induced migration. It was also found that AuNPs remained the same size even after harsh etching and calcination treatment. In a control experiment, AuNP/*m*-TiO_2 hollow spheres were synthesized under similar conditions without the introduction of GO. It was clearly seen that AuNPs aggregated to form large particles (Figure S3). As a result, it is concluded that the presence of GO can effectively prohibit the aggregation of AuNPs during etching and calcination processes possibly due to its strong affinity toward AuNPs.

3.2. Characterization of r-GO/AuNP/*m*-TiO_2 Hollow Spheres. From the XRD pattern of r-GO/AuNP/*m*-TiO_2 hollow hybrids as shown in Figure 3a, all the identified peaks for TiO_2 were assigned to anatase (JCPDS, no. 73−1764). The average crystal size of TiO_2 in r-GO/AuNP/*m*-TiO_2 hollow hybrids is approximately 3 nm as calculated from the most intensive (101) peaks based on the Scherrer formula. Besides, additional peaks corresponding to Au have also been observed. Note that a broad diffraction peak at around 26° corresponding

DOI: 10.1021/acsami.5b00663
ACS Appl. Mater. Interfaces 2015, 7, 6909−6918

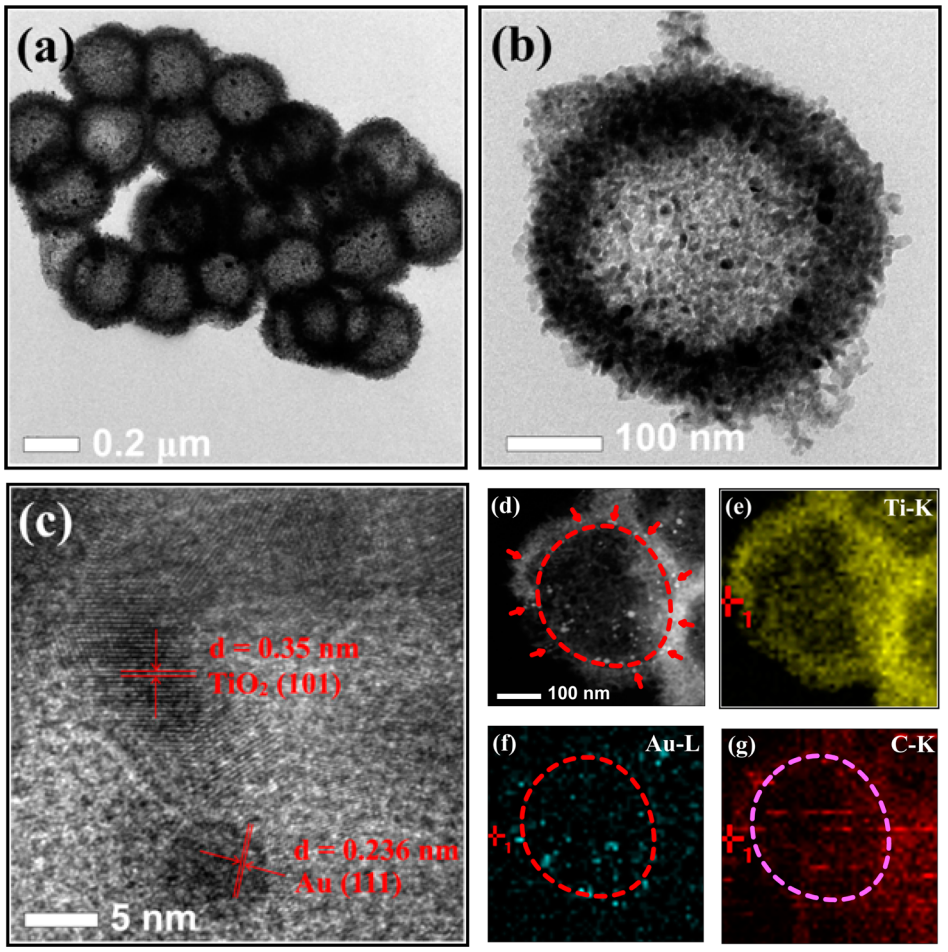

Figure 2. (a, b) TEM and (c) HRTEM images of r-GO/AuNP/*m*-TiO_2 hollow spheres. (d) HAADF-STEM image of r-GO/AuNP/*m*-TiO_2 hollow spheres and (e, f) EDS maps of (e) Ti, (f) Au, and (g) C from a single particle given in Figure 1d.

to r-GO was not observed in the XRD pattern due to the strong diffraction from crystalline TiO_2. In the XPS spectrum of r-GO/AuNP/*m*-TiO_2 hollow hybrids (Figure S4), only the signatures of Ti, O for TiO_2, and Au, C for Au and r-GO can be evidenced. The XPS signature of Au 4f doublet peaks (Figure 3b) for AuNPs locate at 82.3 and 86.0 eV with the splitting of the 4f doublet 3.7 eV, suggesting the metallic nature of Au. However, the peaks show a large shift to the direction of low energy according to the XPS handbooks and the previous reports.[30] For comparison, XPS spectra of GO/AuNP/TiO_2 hollow hybrids (before calculation for r-GO/AuNP/*m*-TiO_2 hollow hybrids) were also recorded, where the Au 4f doublet peaks for AuNPs in GO/AuNP/TiO_2 hollow hybrids were located at 83.8 and 87.5 eV. In addition, the Ti 2p doublet peaks for TiO_2 in GO/AuNP/TiO_2 are located at 459.0 and 464.8 eV, whereas those in r-GO/AuNP/*m*-TiO_2 hollow hybrids locate at 457.8 and 463.5 eV, both with the splitting of the 2p doublet 5.7 eV (Figure 3c), suggesting a normal state of Ti^{4+}. In addition, the Au 4f and Ti 2p binding energy shows 1.3 and 1.2 eV shifts, respectively, both in the direction of low energy. Figure 3d shows the C 1s peaks of GO and r-GO/AuNP/*m*-TiO_2 hollow hybrids. A high ratio of nonoxygenated C to the carbonyl C in r-GO/AuNP/*m*-TiO_2 hollow hybrids can be evidenced, suggesting a considerable degree of reduction for the GO nanosheets.[31] The shift of Au 4f indicates that some electrons may migrate from TiO_2 to metallic Au and there is a strong interaction between AuNPs and TiO_2. Because AuNPs can act as electron acceptors and help to separate the photoexcited electron−hole pairs, the hybrid structure can inhibit the recombination of excited electrons and holes. The shifts of 1.2 eV for Ti 2p may be attributed to the interactions of Ti with oxygen centers of r-GO. It is noted that a slight shift to lower binding energy is observed for the peaks of the C 1s spectra after the thermal treatment, suggesting the formation of Ti−O−C bonds between TiO_2 and r-GO after high temperature annealing.[32−35] The above results indicate that strong interactions in the ternary hybrids can be verified.

The surface area and porosity of r-GO/AuNP/*m*-TiO_2 hollow hybrids were measured by N_2 adsorption−desorption isotherm analysis, with the results shown in Figure 3e. The isotherm is of the typical type III pattern with H_3 hysteretic loop in the range of 0.5−1.0 P/P_0, indicating the existence of slit-shaped pores according to the IUPAC classification. The surface area as measured by the multipoint BET method from the adsorption branch is 171.4 $m^2\ g^{-1}$, which is much higher than commercial P25 (about 50 $m^2\ g^{-1}$). The pore size distribution of the sample as determined using the BJH method from the adsorption branch of the isotherm is shown in the inset in Figure 3e, which suggests an average pore diameter of 6.0 nm.

The UV/vis diffuse reflectance spectra were conducted to uncover the optical properties of r-GO/AuNP/*m*-TiO_2 hollow hybrids (Figure 4a). The addition of r-GO induced the increased light absorption intensity in visible light regions, as

DOI: 10.1021/acsami.5b00663
ACS Appl. Mater. Interfaces 2015, 7, 6909−6918

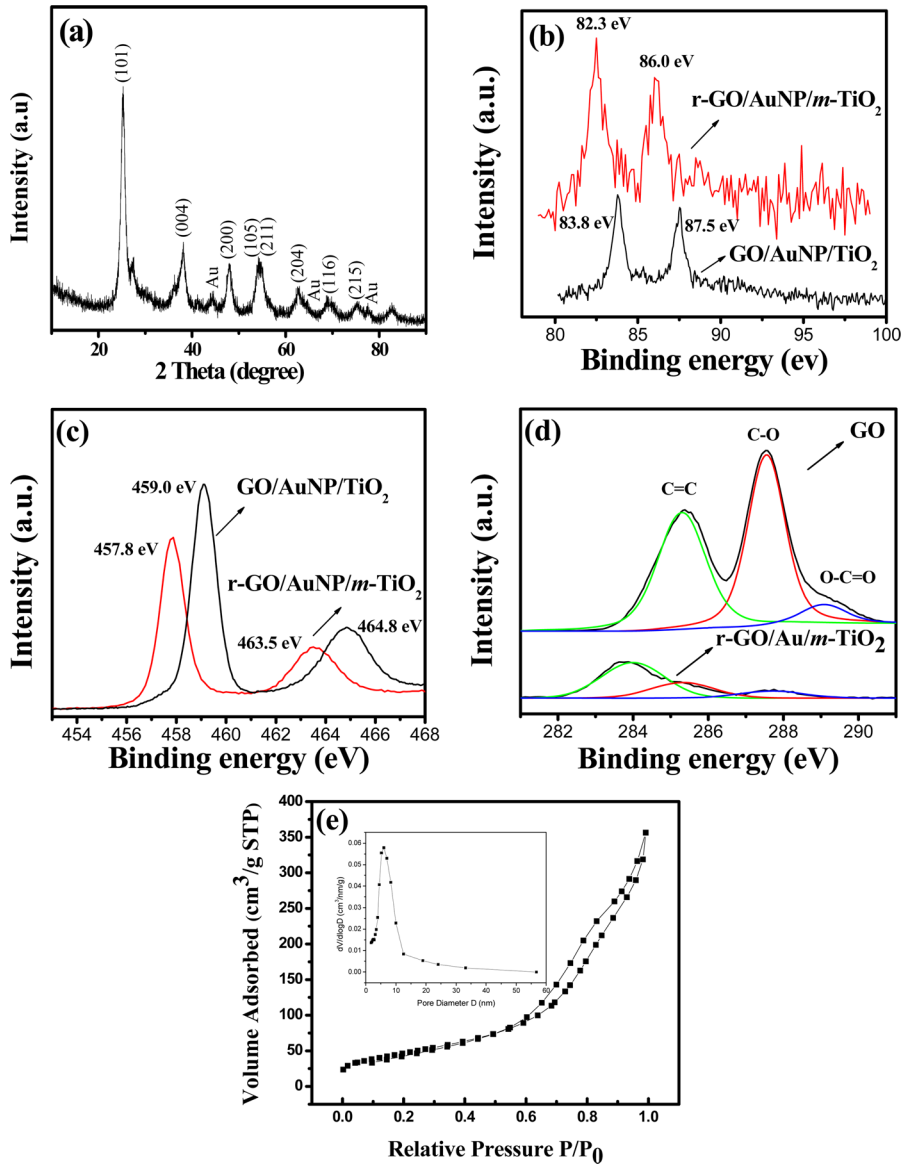

Figure 3. (a) XRD pattern of r-GO/AuNP/*m*-TiO_2 hollow hybrids. (b–d) XPS spectra of (b) Au 4f, (c) Ti 2p, and (d) C 1s. (e) Nitrogen adsorption isotherm of r-GO/AuNP/*m*-TiO_2 hollow hybrids. Inset in Figure 2e shows the pore size distribution as calculated by using the BJH method.

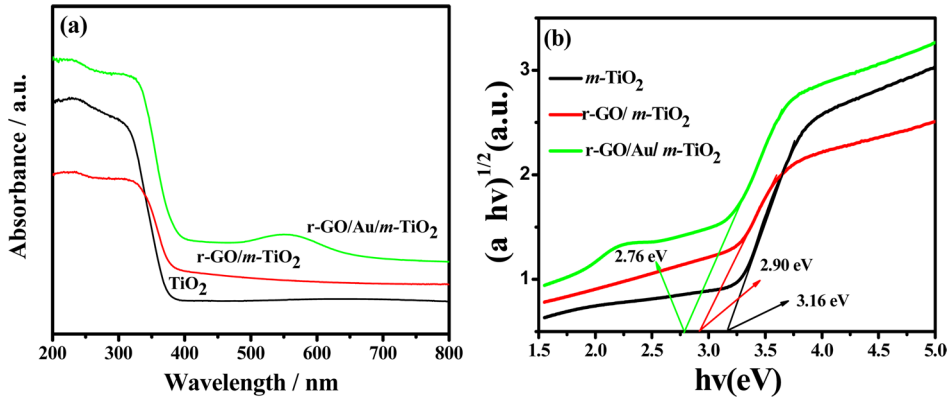

Figure 4. (a) UV/vis diffuse reflectance spectra of *m*-TiO_2, r-GO/*m*-TiO_2, and r-GO/AuNP/*m*-TiO_2 hollow spheres and (b) their corresponding Kubelka–Munk plots.

compared to the bare *m*-TiO_2. Moreover, another absorption band for r-GO/AuNP/*m*-TiO_2 hollow hybrids at around 550 nm appeared, which could be ascribed to the surface plasmon resonance of AuNPs. Furthermore, a qualitative red shift to

DOI: 10.1021/acsami.5b00663
ACS Appl. Mater. Interfaces 2015, 7, 6909–6918

longer wavelength is also observed in the absorption edge. Figure 4b shows the plots of the Kubelka–Munk remission function corresponding to each spectrum, which indicates that bare anatase m-TiO_2 was 3.16 eV, while the band gap of the r-GO/m-TiO_2 estimated from the spectrum was 2.90 eV, and the band gap of the r-GO/Au/m-TiO_2 hollow spheres were significantly reduced to 2.76 eV. This phenomenon should occur due to the interaction between graphene and TiO_2 and the surface plasmon resonance of AuNPs.[36]

On the basis of above results, the morphology and chemical structures of r-GO/AuNP/m-TiO_2 hollow hybrids can be successfully verified. It is believed that the mesoporous shells with large surface area and enhanced visible absorption may potentially promote their photocatalytic performance.

3.3. Catalytic Activities of r-GO/AuNP/m-TiO_2 Photocatalysts in the Degradation of RhB. The activity of r-GO/AuNP/m-TiO_2 photocatalysts was evaluated by monitoring the photodegradation of RhB under different light irradiation. Before light irradiation, the solution containing catalysts and dyes was stirred in the dark for 30 min to ensure equilibrium adsorption of RhB on surfaces of catalysts. As shown in Figure 5, m-TiO_2 hollow spheres show higher adsorptivity than commercial TiO_2 and P25. In addition, the introduction of r-GO and AuNPs in mesoporous hollow TiO_2 can significantly increase the adsorptivity of RhB, which can reach as high as 34% for r-GO/AuNP/m-TiO_2. It is possible that the introduction of AuNPs in r-GO/m-TiO_2 will create more nanopores between r-GO and m-TiO_2 in the hybrid shells, leading to better adsorptivity than r-GO/m-TiO_2.

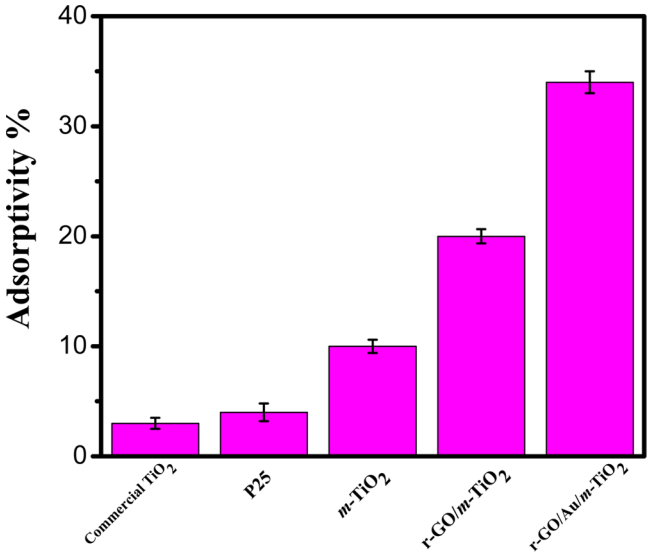

Figure 5. Bar plot showing the adsorptivity of RhB with different photocatalysts.

The performance of r-GO/AuNP/m-TiO_2 photocatalysts toward the rate of RhB degradation was measured by monitoring the adsorption intensity of the characteristic RhB peak at 553 nm. For comparison, the degradation of RhB with commercial TiO_2, P25, m-TiO_2 and r-GO/m-TiO_2 photocatalysts was also measured. Figure 6a shows time profiles of C_t/C_0 under UV irradiation, where C_t is the concentration of RhB at irradiation time t and C_0 the concentration at absorption equilibrium of the photocatalyst before irradiation. It is clear that m-TiO_2 hollow spheres show higher degradation efficiency than commercial TiO_2 and P25 possibly due to their large surface area, superior adsorption ability, and possible light-trapping effect resulting from mesoporous shells. Considering the electric conductivity and visible light absorption of r-GO, it is not surprising that the introduction of r-GO to m-TiO_2 can enhance the degradation efficiency. More interestingly, the presence of AuNPs in r-GO/AuNP/m-TiO_2 could further improve their degradation efficiency with the rate constant reaching as high as 1.02 min^{-1} (Figure 6b), which is believed to surpass most of the reported TiO_2-based photocatalysts (Table 1). The results undoubtedly confirm the positive impact of r-

Table 1. Comparison of the Photocatalytic Activity of Different TiO_2-Based Photocatalysts

sample	k (min^{-1})	irradiation	organic dye	ref
TiO2-PE-800	0.15	UV	RhB	15
TiO_2 hollow spheres	0.013	UV	MB	37
graphene/TiO_2 mixture	0.20	UV	RhB	38
H-TiO_2-800	0.20	UV	RhB	16
Au-TiO_2 nanocups	0.022	UV	MB	12
$Fe_3O_4/SiO_2/TiO_2$	0.17	UV	RhB	39
TiO_2/TiO_2	0.0034	UV	MO	40
Au@TiO_2 core/shell	0.0087	UV	RhB	41
m-TiO_2	0.32	UV	RhB	this work
r-GO/m-TiO_2	0.73	UV	RhB	this work
r-GO/AuNP/m-TiO_2	1.02	UV	RhB	this work

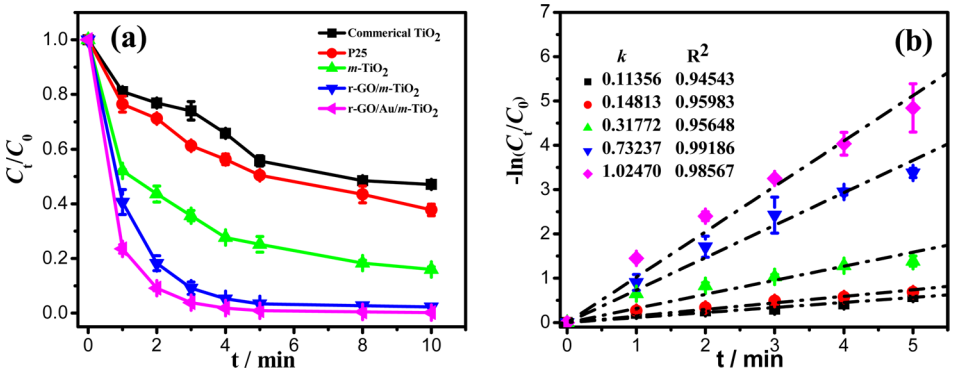

Figure 6. (a) Evolution of RhB concentration versus reaction time under UV irradiation and (b) apparent reaction rate constant versus UV irradiation time in the presence of different photocatalysts.

DOI: 10.1021/acsami.5b00663
ACS Appl. Mater. Interfaces 2015, 7, 6909–6918

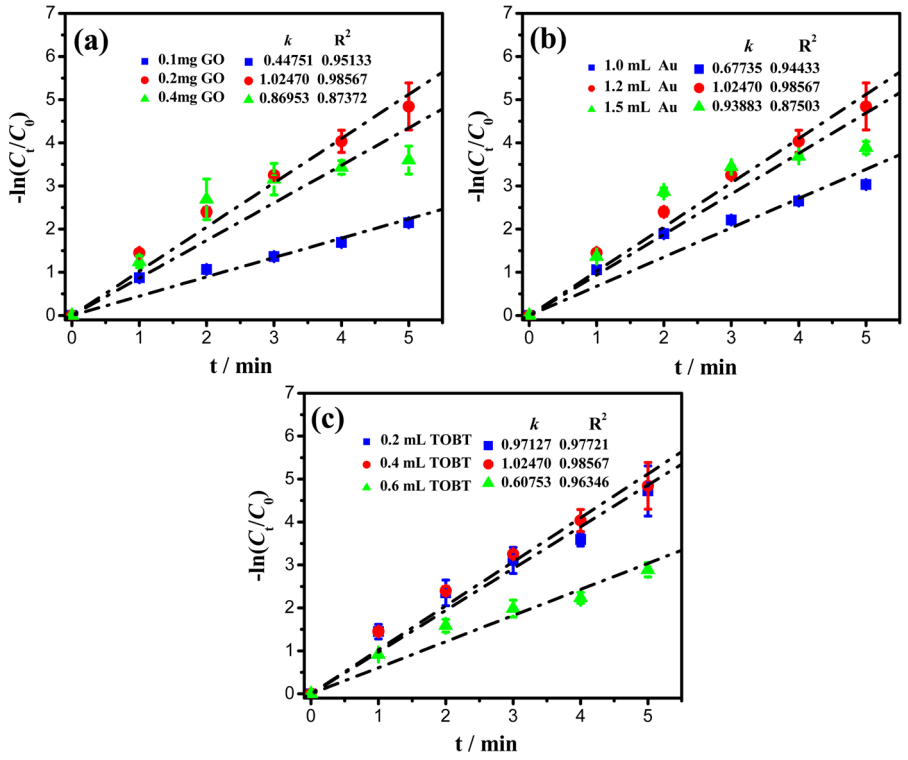

Figure 7. Apparent reaction rate constant versus reaction time under UV irradiation in the presence of r-GO/AuNP/*m*-TiO_2 with different amount of (a) GO, (b) Au, and (c) TOBT as the photocatalysts.

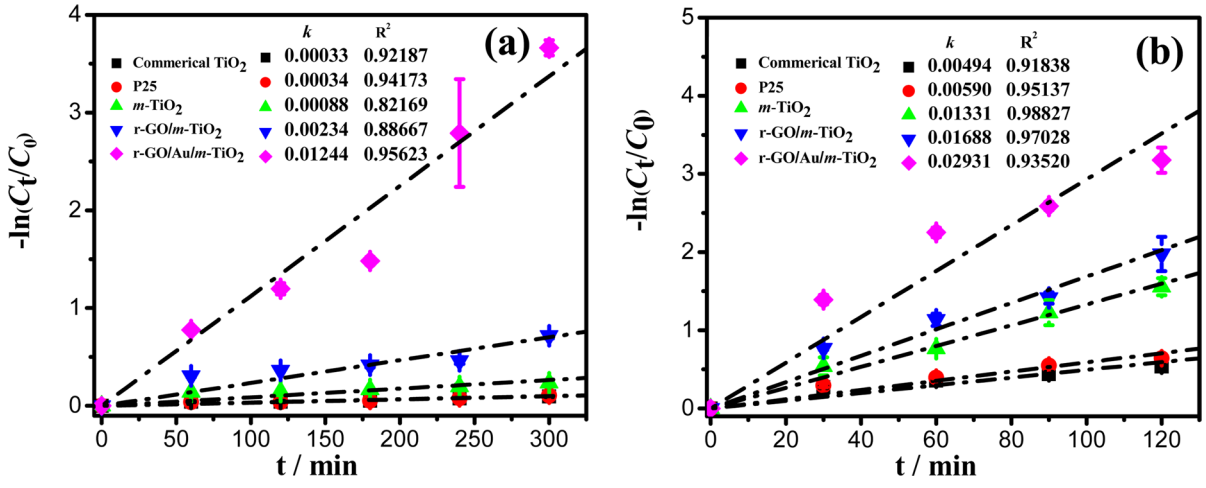

Figure 8. Apparent reaction rate constant versus (a) visible light and (b) simulated daylight irradiation time in the presence of different photocatalysts.

GO and Au decoration on catalytic activity. It is found that r-GO/AuNP/*m*-TiO_2 photocatalysts are also mechanically robust and chemically stable: they can be recovered and reused to catalyze multiple cycles of degradation reactions under UV light irradiation (Figure S5). In addition, r-GO/AuNP/*m*-TiO_2 hollow hybrids were also active photocatalysts for degradation of other organic dyes, such as methylene blue (MB) and methyl orange (MO) (Figure S6).

The structures of r-GO/AuNP/*m*-TiO_2 hollow hybrids were also optimized by varying the compositions to assess the effect of different ingredients in catalytic efficiency. It was found that higher r-GO amount in r-GO/AuNP/*m*-TiO_2 hollow hybrids led to decreased photocatalytic activity as shown in Figure 7a and Figure S7a, which was consistent with reported results.[24,31,42] The increasing coverage of r-GO on TiO_2 with higher r-GO amount will facilitate faster photodegradation due to electric conductivity and visible light absorption of r-GO; however, excessive r-GO not hybridized with TiO_2 should be accounted for the decreased photocatalytic activity.[41] As for AuNP, it is generally understood that AuNPs can help to enhance charge separation by serving as an electron reservoir, and to act as a recombination center which negatively affects catalytic activity.[21] Therefore, excessive amounts of AuNPs may increase the occurrence of exciton recombination,[21,43] which leads to decreased photocatalytic activity (Figure 7b and Figure S7b). Figure 7c and Figure S7c reveal the photocatalytic activity variation with TBOT amount. It was found that the TiO_2 shell thickness increased with increasing TBOT amount. The

DOI: 10.1021/acsami.5b00663
ACS Appl. Mater. Interfaces 2015, 7, 6909−6918

increase in TiO_2 shell thickness may lead to increased migration distance of photoexcited electrons/holes to the catalyst surfaces, which is believed to diminish the photocatalytic activity. Hereafter, the optimized r-GO/AuNP/*m*-TiO_2 hollow hybrids were chosen as photocatalysts in visible light and simulated daylight irradiation experiments.

For the visible light irradiation experiment, a 400 W metal halide lamp was used as the light source, and a cutoff filter was used to block the UV light (<400 nm). As shown in Figure S8a, r-GO/AuNP/*m*-TiO_2 photocatalysts can decompose more than 97% of RhB within 5 h, while commercial TiO_2 and P25 containing an equivalent amount of TiO_2 can convert only about 10% of RhB under identical photodegradation conditions. The relative photocatalytic activity of the catalysts for RhB degradation follows the order r-GO/AuNP/*m*-TiO_2 > r-GO/*m*-TiO_2 > *m*-TiO_2 > P25 > commercial TiO_2 (Figure 8a), which is similar to the trends under conditions of UV light irradiation. A 350 W xenon lamp was used as the light source to simulate daylight irradiation. As shown in Figure S8b, approximately 96.4% of RhB was degraded within 2 h by r-GO/AuNP/*m*-TiO_2 photocatalysts; the value can reach as high as 99.7% when the irradiation time is prolonged to 2.5 h. The relative photocatalytic activity of the catalysts for RhB degradation follows the same order as in the cases of UV and visible light irradiation (Figure 8b).

From the above results, we can conclude that the introduction of r-GO and AuNPs can significantly enhance the photocatalytic performances of *m*-TiO_2 in degradation of RhB under UV, visible light, and simulated daylight conditions. It is known that typical photocatalytic decomposition of organic pollutant species involves three main steps: adsorption of the organic molecules, absorption of light by the photocatalyst, and charge transfer reactions to create the oxidative radical species to decompose the pollutants. Upon irradiation of r-GO/AuNP/*m*-TiO_2 with UV light, electrons are excited from the VB to the CB of TiO_2 generating holes in the VB. Photoexcited electrons and holes can then react with H_2O and/or dissolved oxygen to create oxidative radicals which can undergo chain reactions to decompose the organic pollutants into small molecules.[44] It is known that the fast intrinsic electron/hole pair recombination results in low catalytic activity. The incorporation of graphene in fact as a bridge for the electron transfer, which largely enhances the transition probability of the valence in TiO_2 to its conduction band, resulting in an increase in photoconduction that is conducive to reduction of the photogenerated carrier recombination rate, and the presence of AuNPs is believed to enhance charge separation by serving as an electron reservoir. Under visible light irradiation, AuNPs in hybrid shells help to harvest the visible-light energy through plasmonic excitation in the visible spectrum, and then charge separation is finished by transfer of electrons from AuNPs to CB of TiO_2. At the same time, the CB electrons of the TiO_2 transfer to r-GO as the mobility of these electrons on r-GO sheets is high due to their unique electric property. The r-GO in the hollow hybrids can behave as photoelectron reservoirs,[32−35] while under simulated daylight irradiation, it may collect both UV and visible light reaction mechanisms: electrons excited from the VB to the CB of TiO_2, together with electrons from AuNPs due to plasmonic excitation are both transferred to r-GO. The electrochemical impedance spectra were presented as Nyquist plots (Figure 9), in which r-GO/AuNP/*m*-TiO_2 showed the smallest semicircle in the middle-frequency region, followed by r-GO/*m*-TiO_2 and *m*-TiO_2. The results indicate reduced charge transfer resistance

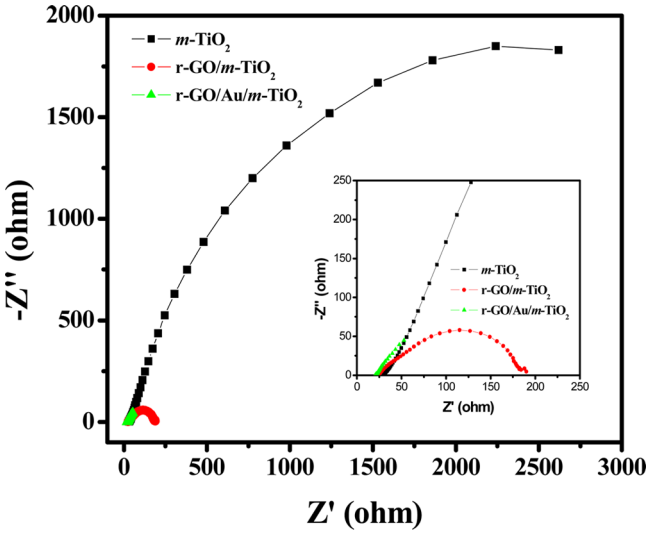

Figure 9. Nyquist plots of *m*-TiO_2, r-GO/*m*-TiO_2, and r-GO/AuNP/*m*-TiO_2 in 0.5 mol/L Na_2SO_4 aqueous solution.

in the solid state interface after the introduction of r-GO,[45,46] and the addition of AuNPs further deepen the impact. Therefore, the electron accepting and transporting properties of r-GO and AuNPs in r-GO/AuNP/*m*-TiO_2 hollow hybrids can contribute to the suppression of charge recombination, and thereby result in high photocatalytic performance. In addition, the large surface area of r-GO/AuNP/*m*-TiO_2 hollow hybrids with improved dye adsorption may facilitate the transfer of photogenerated excitons to dyes, which also leads to increased photocatalytic activity.

4. CONCLUSION

We report in this work the successful fabrication of sandwich-structured r-GO/AuNP/*m*-TiO_2 hollow hybrid shells with large surface area and superior adsorption ability via the combination of sol−gel and self-assembly methods. Results on photocatalytic degradation of RhB indicated that the introduction of r-GO and AuNPs could improve the catalytic activity of *m*-TiO_2. The superior photocatalytic performance of r-GO/AuNP/*m*-TiO_2 hollow hybrids as revealed by RhB degradation under both UV and visible irradiation clearly suggested their potential application as powerful photocatalysts. We believe the strategy developed here is instructive for construction of other sandwich-structured r-GO/noble metal/*m*-TiO_2 hollow hybrid shells for broader applications such as photocatalysts for water splitting, active layers for hybrid solar cells, and electrode materials for lithium ion batteries.

■ ASSOCIATED CONTENT

Ⓢ Supporting Information

Additional figures giving detailed material characterizations. This material is available free of charge via the Internet at http://pubs.acs.org.

■ AUTHOR INFORMATION

Corresponding Authors

*E-mail: hanjie@yzu.edu.cn.
*E-mail: yadong.yin@ucr.edu.

Notes

The authors declare no competing financial interest.

DOI: 10.1021/acsami.5b00663
ACS Appl. Mater. Interfaces 2015, 7, 6909−6918

■ ACKNOWLEDGMENTS

The authors gratefully acknowledge financial support from the National Natural Science Foundation of China (No. 21273004 and 41472034), Research Fund for the Doctoral Program of Higher Education of China (20113250110007), and the Priority Academic Program Development of Jiangsu Higher Education Institutions. We would also like to acknowledge the technical support received at the Testing Center of Yangzhou University. Yin also thanks the financial support by the U.S. Department of Energy (DE-FG02-09ER16096).

■ REFERENCES

(1) Fujishima, A.; Honda, K. Electrochemical Photolysis of Water at a Semiconductor Electrode. *Nature* **1972**, *238*, 37−38.
(2) Kudo, A.; Miseki, Y. Heterogeneous Photocatalyst Materials for Water Splitting. *Chem. Soc. Rev.* **2009**, *38*, 253−278.
(3) Girish, S.; Devi, L. G. Review on Modified TiO_2 Photocatalysis under UV/Visible Light: Selected Results and Related Mechanisms on Interfacial Charge Carrier Transfer Dynamics. *J. Phys. Chem. A* **2011**, *115*, 13211−13241.
(4) Tong, H.; Ouyang, S.; Bi, Y.; Umezawa, N.; Oshikiri, M.; Ye, J. Nano-photocatalytic Materials: Possibilities and Challenges. *Adv. Mater.* **2012**, *24*, 229−251.
(5) Li, W.; Wu, Z.; Wang, J.; Elzatahry, A. A.; Zhao, D. A Perspective on Mesoporous TiO_2 Materials. *Chem. Mater.* **2014**, *26*, 287−298.
(6) Henderson, M. A.; Lyubinetsky, I. Molecular-Level Insights into Photocatalysis from Scanning Probe Microscopy Studies on TiO_2 (110). *Chem. Rev.* **2013**, *113*, 4428−4455.
(7) Balasanthiran, C.; Hoefelmeyer, J. D. Facile Method to Attach Transition Metal Ions to The Surface of Anatase TiO_2 Nanorods. *Chem. Commun.* **2014**, *50*, 5721−5724.
(8) Lu, Q.; Lu, Z.; Lu, Y.; Lv, L.; Ning, Y.; Yu, H.; Hou, Y.; Yin, Y. Photocatalytic Synthesis and Photovoltaic Application of Ag-TiO_2 Nanorod Composites. *Nano Lett.* **2013**, *13*, 5698−5702.
(9) Naito, K.; Tachikawa, T.; Fujitsuka, M.; Majima, T. Single-Molecule Observation of Photocatalytic Reaction in TiO_2 Nanotube: Importance of Molecular Transport through Porous Structures. *J. Am. Chem. Soc.* **2009**, *131*, 934−936.
(10) Huang, Z.; Wang, Z.; Lv, K.; Zheng, Y.; Deng, K. Transformation of $TiOF_2$ Cube to a Hollow Nanobox Assembly from Anatase TiO_2 Nanosheets with Exposed {001} Facets via Solvothermal Strategy. *ACS Appl. Mater. Interfaces* **2013**, *5*, 8663−8669.
(11) Shang, S.; Jiao, X.; Chen, D. Template-Free Fabrication of TiO_2 Hollow Spheres and Their Photocatalytic Properties. *ACS Appl. Mater. Interfaces* **2012**, *4*, 860−865.
(12) Lu, J. W.; Zhang, P.; Li, A.; Su, F. L.; Wang, T.; Liu, Y.; Gong, J. L. Mesoporous Anatase TiO_2 Nanocups with Plasmonic Metal Decoration for Highly Active Visible-Light Photocatalysis. *Chem. Commun.* **2013**, *49*, 5817−5819.
(13) Jiao, W.; Wang, L.; Liu, G.; Lu, G. Q.; Cheng, H. M. Hollow Anatase TiO_2 Single Crystals and Mesocrystals with Dominant {101} Facets for Improved Photocatalysis Activity and Tuned Reaction Preference. *ACS Catal.* **2012**, *2*, 1854−1859.
(14) Joo, J.; Zhang, Q.; Lee, I.; Dahl, M.; Zaera, F.; Yin, Y. Mesoporous Anatase Titania Hollow Nanostructures though Silica-Protected Calcination. *Adv. Funct. Mater.* **2012**, *22*, 166−174.
(15) Joo, J.; Zhang, Q.; Dahl, M.; Lee, I.; Goebl, J.; Zaera, F.; Yin, Y. Control of the Nanoscale Crystallinity in Mesoporous TiO_2 Shells for Enhanced Photocatalytic Activity. *Energy Environ. Sci.* **2012**, *5*, 6321−9327.
(16) Joo, J. B.; Dahl, M.; Li, N.; Zaera, F.; Yin, Y. Tailored Synthesis of Mesoporous TiO_2 Hollow Nanostructures for Catalytic Applications. *Energy Environ. Sci.* **2013**, *6*, 2082−2092.
(17) Li, Y. F.; Xu, D.; Oh, J. I.; Shen, W.; Li, X.; Yu, Y. Mechanistic Study of Codoped Titania with Nonmetal and Metal Ions: A Case of C+ Mo Codoped TiO_2. *ACS Catal.* **2012**, *2*, 391−398.
(18) Pan, J. H.; Zhang, X. W.; Du, A. J. H.; Sun, D. D.; Leckie, J. O. Self-Etching Reconstruction of Hierarchically Mesoporous F-TiO_2 Hollow Microspherical Photocatalyst for Concurrent Membrane Water Purifications. *J. Am. Chem. Soc.* **2008**, *130*, 11256−11257.
(19) Lei, J. F.; Li, L. B.; Shen, X. H.; Du, K.; Ni, J.; Liu, C. J.; Li, W. S. Fabrication of Ordered ZnO/TiO_2 Heterostructures via a Templating Technique. *Langmuir* **2013**, *29*, 13975−13981.
(20) Naya, S.; Inoue, A.; Tada, H. Self-Assembled Heterosupramolecular Visible Light Photocatalyst Consisting of Gold Nanoparticle-Loaded Titanium(IV) Dioxide and Surfactant. *J. Am. Chem. Soc.* **2010**, *132*, 6292−6293.
(21) Zhang, Q.; Lima, D. Q.; Lee, I.; Zaera, F.; Chi, M.; Yin, Y. A Highly Active Titanium Dioxide Based Visible-Light Photocatalyst with Nonmetal Doping and Plasmonic Metal Decoration. *Angew. Chem., Int. Ed.* **2011**, *50*, 7088−7092.
(22) Xiang, Q.; Yu, J.; Jaroniec, M. Synergetic Effect of MoS_2 and Graphene as Cocatalysts for Enhanced Photocatalytic H_2 Production Activity of TiO_2 Nanoparticles. *J. Am. Chem. Soc.* **2012**, *134*, 6575−6578.
(23) Wang, S.; Yi, L.; Halpert, J. E.; Lai, X.; Liu, Y.; Cao, H.; Yu, R.; Wang, D.; Li, Y. A Novel and Highly Efficient Photocatalyst Based on P25-Graphdiyne Nanocomposite. *Small* **2012**, *8*, 265−271.
(24) Lee, J. S.; You, K. H.; Park, C. B. Highly Photoactive, Low Bandgap TiO_2 Nanoparticles Wrapped by Graphene. *Adv. Mater.* **2012**, *24*, 1084−1088.
(25) Xiang, Q.; Yu, J.; Jaroniec, M. Graphene-Based Semiconductor Photocatalysts. *Chem. Soc. Rev.* **2012**, *41*, 782−796.
(26) Cui, S.; Mao, S.; Lu, G.; Chen, J. Graphene Coupled with Nanocrystals: Opportunities and Challenges for Energy and Sensing Applications. *J. Phys. Chem. Lett.* **2013**, *4*, 2441−2454.
(27) Krishnamurthy, S.; Kamat, P. V. Galvanic Exchange on Reduced Graphene Oxide: Designing a Multifunctional Two-Dimensional Catalyst Assembly. *J. Phys. Chem. C* **2013**, *117*, 571−577.
(28) Kong, B. S.; Geng, J.; Jung, H. T. Layer-by-Layer Assembly of Graphene and Gold Nanoparticles by Vacuum Filtration and Spontaneous Reduction of Gold Ions. *Chem. Commun.* **2009**, 2174−2176.
(29) Wang, J.; Dong, X.; Xu, R.; Li, S.; Chen, P.; Chan-Park, M. B. Template-Free Synthesis of Large Anisotropic Gold Nanostructures on Reduced Graphene Oxide. *Nanoscale* **2012**, *4*, 3055−3059.
(30) Tsunoyama, H.; Sakurai, H.; Ichikuni, N.; Negishi, Y.; Tsukuda, T. Colloidal Gold Nanoparticles as Catalyst for Carbon−Carbon Bond Formation: Application to Aerobic Homocoupling of Phenylboronic Acid in Water. *Langmuir* **2004**, *20*, 11293−11296.
(31) Shah, M. S. A. S.; Park, A. R.; Zhang, K.; Park, J. H.; Yoo, P. J. Green Synthesis of Biphasic TiO_2−Reduced Graphene Oxide Nanocomposites with Highly Enhanced Photocatalytic Activity. *ACS Appl. Mater. Interfaces* **2012**, *4*, 3893−3901.
(32) Wu, Y. M.; Liu, H. B.; Zhang, J. L.; Chen, F. Enhanced Photocatalytic Activity of Nitrogen-Doped Titania by Deposited with Gold. *J. Phys. Chem. C* **2009**, *113*, 14689−14695.
(33) Shah, M. S. A. S.; Park, A. R.; Zhang, K.; Park, J. H.; Yoo, P. J. Green Synthesis of Biphasic TiO_2−Reduced Graphene Oxide Nanocomposites with Highly Enhanced Photocatalytic Activity. *ACS Appl. Mater. Interfaces* **2012**, *4*, 3893−3901.
(34) Gu, L. A.; Wang, J. Y.; Cheng, H.; Zhao, Y. Z.; Liu, L. F.; Han, X. J. One-Step Preparation of Graphene-Supported Anatase TiO_2 with Exposed {001} Facets and Mechanism of Enhanced Photocatalytic Properties. *ACS Appl. Mater. Interfaces* **2013**, *5*, 3085−3093.
(35) Shah, M. S. A. S.; Park, A. R.; Zhang, K.; Park, J. H.; Yoo, P. J. Green Synthesis of Biphasic TiO_2-Reduced Graphene Oxide Nanocomposites with Highly Enhanced Photocatalytic Activity. *ACS Appl. Mater. Interfaces* **2012**, *4*, 3893−3901.
(36) Zhang, H.; Lv, X.; Li, Y.; Wang, Y.; Li, J. P25-Graphene Composite as a High Performance Photocatalyst. *ACS Nano* **2010**, *4*, 380−386.
(37) Tim, L.; Stuart, L.; George, B.; Frank, G. Mesoporous Hollow Sphere Titanium Dioxide Photocatalysts through Hydrothermal Silica Etching. *ACS Appl. Mater. Interfaces* **2012**, *4*, 6062−6070.

DOI: 10.1021/acsami.5b00663
ACS Appl. Mater. Interfaces 2015, 7, 6909−6918

(38) Liang, Y.; Wang, H.; Casalongue, H. S.; Chen, Z.; Dai, H. TiO_2 Nanocrystals Grown on Graphene as Advanced Photocatalytic Hybrid Materials. *Nano Res.* **2010**, *3*, 701−705.
(39) Ye, M.; Zhang, Q.; Hu, X.; Ge, J.; Lu, Z.; He, L.; Chen, Z.; Yin, Y. Magnetically Recoverable Core−Shell Nanocomposites with Enhanced Photocatalytic Activity. *Chem.—Eur. J.* **2010**, *16*, 6243−6250.
(40) Wang, D. P.; Zeng, H. C. Multifunctional Roles of TiO_2 Nanoparticles for Architecture of Complex Core−Shells and Hollow Spheres of SiO_2−TiO_2−Polyaniline System. *Chem. Mater.* **2009**, *21*, 4811−4823.
(41) Zhang, N.; Liu, S.; Fu, X.; Xu, Y. Synthesis of M@TiO_2 (M = Au, Pd, Pt) Core−Shell Nanocomposites with Tunable Photoreactivity. *J. Phys. Chem. C* **2011**, *115*, 9136−9145.
(42) Zhang, Y.; Tang, Z. R.; Fu, X.; Xu, Y. J. TiO_2−Graphene Nanocomposites for Gas-Phase Photocatalytic Degradation of Volatile Aromatic Pollutant: Is TiO_2−Graphene Truly Different from Other TiO2−Carbon Composite Materials? *ACS Nano* **2010**, *4*, 7303−7314.
(43) Wu, Y. M.; Liti, H. B.; Zhang, J. L.; Chen, F. Enhanced Photocatalytic Activity of Nitrogen-Doped Titania by Deposited with Gold. *J. Phys. Chem. C* **2009**, *113*, 14689−14695.
(44) Zhang, L. W.; Fu, H. B.; Zhu, Y. F. Efficient TiO_2 Photocatalysts from Surface Hybridization of TiO_2 Particles with Graphite-like Carbon. *Adv. Funct. Mater.* **2008**, *18*, 2180−2189.
(45) Zhang, Y. H.; Zhang, N.; Tang, Z. R.; Xu, Y. J. Graphene Transforms Wide Band Gap ZnS to a Visible Light Photocatalyst. The New Role of Graphene as a Macromolecular Photosensitizer. *ACS Nano* **2012**, *6*, 9777−9789.
(46) Zhang, N.; Yang, M. Q.; Tang, Z. R.; Xu, Y. J. Toward Improving the Graphene−Semiconductor Composite Photoactivity *via* the Addition of Metal Ions as Generic Interfacial Mediator. *ACS Nano* **2014**, *8*, 623−633.

DOI: 10.1021/acsami.5b00663
ACS Appl. Mater. Interfaces 2015, 7, 6909−6918